ELSEVIER

Biophysical Chemistry 120 (2006) 121 – 134

Biophysical Chemistry

http://www.elsevier.com/locate/biophyschem

Thermodynamically based profiling of drug metabolism and drug–drug metabolic interactions: A case study of acetaminophen and ethanol toxic interaction

Feng Yang, Daniel A. Beard *

Biotechnology and Bioengineering Center, Department of Physiology, Medical College of Wisconsin, 8701 Watertown Plank Road, Milwaukee, WI 53226, United States

Received 14 October 2005; received in revised form 18 October 2005; accepted 21 October 2005
Available online 28 November 2005

Abstract

Drug–drug metabolic interactions can result in unwanted side effects, including reduced drug efficacy and formation of toxic metabolic intermediates. In this work, thermodynamic constraints on non-equilibrium metabolite concentrations are used to reveal the biochemical interactions between the metabolic pathways of ethanol and acetaminophen (*N*-acetyl-*p*-aminophenol), two drugs known to interact unfavorably. It is known that many reactions of these pathways are coupled to the central energy metabolic reactions through a number of metabolites and the cellular redox potential. Based on these observations, a metabolic network model has been constructed and a database of thermodynamic properties for all participating metabolites and reactions has been compiled. Constraint-based computational analysis of the feasible metabolite concentrations reveals that the non-toxic pathways for APAP metabolism and the pathway for detoxifying *N*-acetyl-*p*-benzoquinoneimine (NAPQI) are inhibited by network interactions with ethanol metabolism. These results point to the potential utility of thermodynamically based profiling of metabolic network interactions in screening of drug candidates and analysis of potential toxicity.

Keywords: Computational model; Drug metabolism; Drug–drug interaction; Network thermodynamics; Acetaminophen hepatotoxicity

1. Introduction

As one of the most commonly used over-the-counter medications, acetaminophen (APAP) is used for the relief of fever, headaches, or other minor pains. It is also a major ingredient in many cold and flu medications. Although it is generally considered non-toxic at the therapeutic dose, APAP overdose can cause severe liver damage [1]. In certain circumstances, such as fasting or alcohol and other drug use, even a therapeutic dose can cause hepatotoxicity [2].

The coupled metabolism of acetaminophen and ethanol has been studied, both as a clinically important case of potentially toxic drug interaction and as a canonical example of drug–drug interactions [3]. Although the major metabolic pathways have been elucidated, complex interaction mechanisms between these pathways remain an active research subject [4]. Metabolic interactions between APAP and alcohol are complicated because acute and chronic alcohol intakes can have opposite effects [3]; one causes serious hepatocellular injury and the other can actually protect against APAP-induced toxicity. A thorough mechanistic understanding of APAP-induced hepatotoxicity is yet to be established. Clinical and animal-model studies typically use controlled experiments to focus on one or a few aspects of these toxic interactions. Therefore, the scope of these studies is limited in their ability to deduce large-scale network interactions. Here, we construct a network model to systemically study the interactions in APAP-induced hepatotoxicity.

Lacking detailed kinetic information for all of the reactions involved in the network, we postulate that exploration of the thermodynamically feasible fluxes and concentration ranges will reveal global network-scale interactions. The metabolic reaction network reveals that the major reactions of APAP and ethanol metabolism are coupled to the reactions of central energy metabolism through a number of metabolites, such as glutathione, glucose-1-phosphate, acetyl coenzyme A, L-cysteine,

* Corresponding author. Tel.: +1 414 456 5752; fax: +1 414 456 6568.
E-mail address: dbeard@mcw.edu (D.A. Beard).

0301-4622/$ - see front matter © 2005 Elsevier B.V. All rights reserved.
doi:10.1016/j.bpc.2005.10.013

glutamate, 3-phosphoglycerate, alpha-ketoglutarate, and the cellular redox potential. The large number of common species suggests many potential interactions between enzymes and pathways. Although detailed kinetic data are not available, the thermodynamic data for many network reactions are tabulated [5,6]. Given the thermodynamic constraints on the reactant concentrations, and a set of physiological conditions derived from prior knowledge of the concentration pools, we are able to compute the feasible ranges of reactant concentration within the metabolic network. A set of steady-state concentrations is chosen from within the feasible spaces based on a hypothetical objective function that optimizes the stability of the network in response to the perturbations in available substrate concentrations. The utility of this hypothetical objective function is verified by comparison of computational predictions to the experimental data, and by the ability of the model to predict the mechanism and behavior of APAP–ethanol toxic metabolic interactions.

2. Methods

This section is organized as follows. In Section 2.1, the biochemical network for APAP and ethanol metabolism is constructed, and intermediate metabolites directly shared among APAP, ethanol and energetic pathways are identified. A thermodynamic database for all participating metabolites and reactions is compiled in Section 2.2. Thermodynamic and physiological constraints are introduced in Section 2.3. Finally, an additional constraint based on system stability is introduced, and a computational algorithm for predictions of metabolic interactions is detailed in Section 2.4.

2.1. Biochemical network

Developing a biochemical network that captures the essential interacting components of the system is crucial to the analysis of ethanol and APAP metabolism and their metabolic interactions. Reactions involving these species in humans are known; the complete metabolic network analyzed in this work is illustrated in Fig. 1 and tabulated in Table 1. Note that membrane transporters are represented by arrows traversing different compartments in Fig. 1. In addition, the nomenclature and symbols used in Table 1 follow the work of Alberty and Goldberg et al. on which this work is in part built [5,6]. A glossary of major abbreviations used for species names is given in Table 2. The notation "[m]" denotes species present

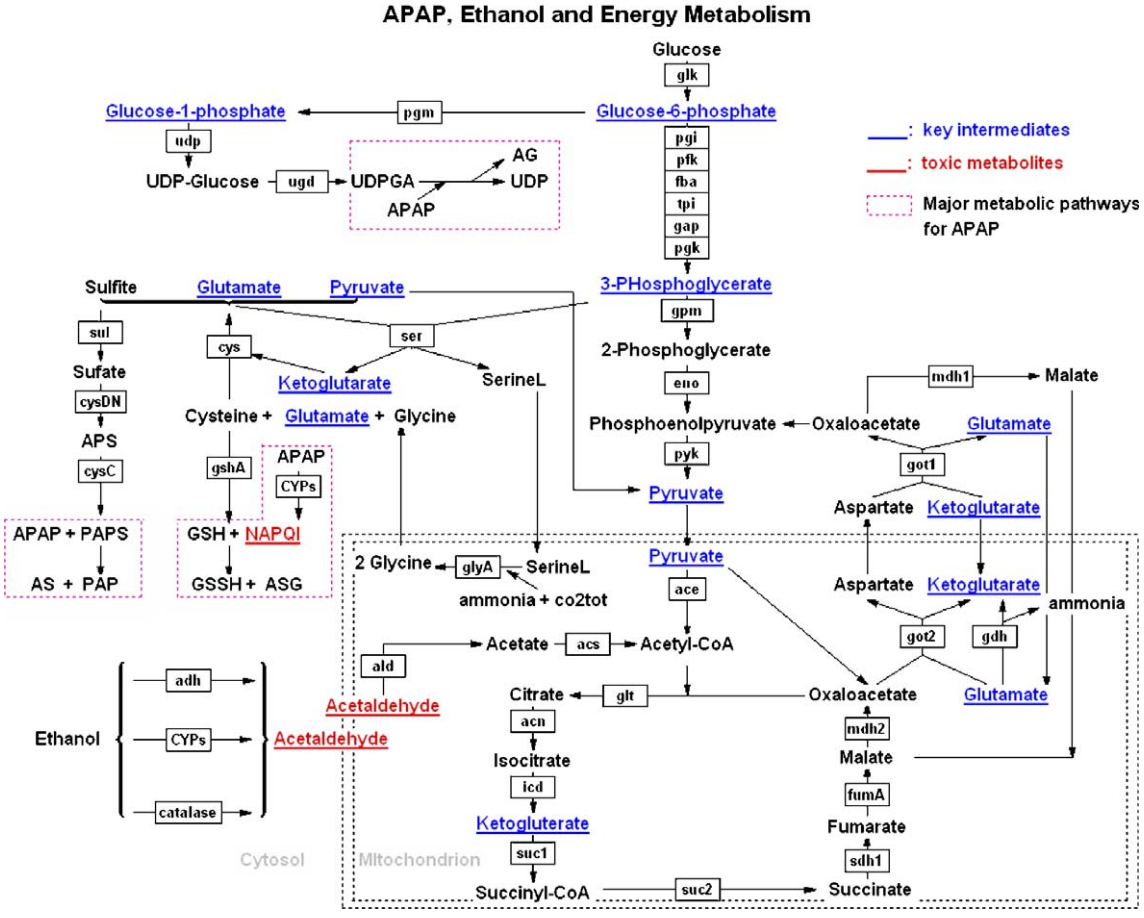

Fig. 1. Reaction network for APAP, ethanol and energy metabolism. The major metabolic pathways are illustrated in this diagram, including the reactions in cytosol and mitochondria. The full network consists of 85 reactants and 80 reactions, although certain metabolites such as NAD(H) and ATP/ADP are not illustrated in this diagram. Gene identifier abbreviations for participating enzymes are listed in the boxes. Network diagram is constructed using the software GenMAPP (www.GenMAPP.org).

in the mitochondrial compartment, and "[c]" denotes species in the cytosol.

2.1.1. Acetaminophen and related metabolism

APAP is metabolized primarily in the liver through three major pathways: (1) conjugation with UDPGA (UDP-glucuronic acid); (2) conjugation with activated sulfate—PAPS (3′-phosphoadenylyl-sulfate); and (3) conjugation with reduced glutathione (GSH) via the hepatic cytochrome *P*450 enzyme system. The resulting conjugate products are inactive compounds that are eventually excreted in bile or urine. The reactions of these three pathways are listed in Table 1 under the heading of "APAP metabolism".

At therapeutic doses (about 0.1 mM), approximately 95% of APAP is conjugated via the glucuronide and sulfate routes and less than 5% is metabolized by the P450 enzyme system—primarily by CYP2E1. However, both glucuronide and sulfate pathways are capacity-limited and easily saturated. Moreover, the sulfation pathway is more important than the glucuronide pathway at therapeutic doses of APAP. In contrast, the glucuronidation pathway becomes relatively more important in the case of APAP overdose. Although only a small fraction of APAP is metabolized by hepatic CYPs, this pathway plays a significant role in APAP-induced hepatotoxicity. The metabolism of APAP by CYPs leads to a toxic reactive oxidizing metabolite, *N*-acetyl-*p*-benzoquinoneimine (NAPQI), which can covalently bind to sulfhydryl groups on hepatic cellular proteins, resulting in widespread hepatocyte damage [4]. Note that cytochrome *P*450 enzyme system is shared by both APAP metabolism and ethanol metabolism. Studies shows that this fact may account for some aspects of the interactions between APAP and ethanol [1,4].

Because UDPGA, PAPS and GSH are the major substrates metabolizing APAP, analyzing their biosyntheses may unveil the toxic interactions between APAP and ethanol. UDPGA biosynthesis is integrated with energy metabolism through glucose-1-phosphate, glucose-6-phosphate, UDP, UTP, PPI, Pi and UPDG (see Fig. 1). The syntheses of PAPS and GSH are tightly integrated because they share the common precursor, L-cysteine. Their synthetic pathways also interact with energy metabolism through glucose-1-phosphate, pyruvate, L-cysteine, glutamate, 3-phosphoglycerate (3pg) and alpha-ketoglutarate.

In certain cases where intermediate species are not directly involved in other reactions in the network, several reactions have been collapsed into an overall reaction. For example in Table 1, the overall reaction for glycine biosynthesis (reaction number 22) is expressed as:

$$\begin{aligned}&\text{ammonia[c]} + \text{co2tot[c]} + \text{nadred[m]} + \text{serineL[m]}\\ &= 2\text{glycine[m]} + \text{h2o[c]} + \text{nadox[m]}.\end{aligned} \tag{1}$$

This overall reaction combines two reactions—glycine hydroxymethyltransferase

$$\begin{aligned}\text{serineL[m]} + \text{THF[m]} &= \text{methylene} - \text{THF[m]}\\ &\quad + \text{glycine[m]} + \text{h2o[c]},\end{aligned} \tag{2}$$

and glycine cleavage,

$$\begin{aligned}&\text{methylene} - \text{THF[m]} + \text{co2tot[c]} + \text{ammonia[c]} + \text{nadred[m]}\\ &= \text{glycine[m]} + \text{THF[m]} + \text{nadox[m]}.\end{aligned} \tag{3}$$

It is possible to combine these reactions because both THF[m] (tetrahydrofolate) and methylene-THF[m] are not involved in the remaining parts of the network. Similarly, glutathione biosynthesis, L-cysteine degradation and serine biosynthesis listed in Table 1 all represent simplified overall reactions. Here, the biosynthesis of L-cysteine is not considered because its synthetic reactions are not closely connected with APAP metabolism. Therefore, instead of including the details of L-cysteine synthesis, which uses methionine as a precursor, this analysis fixes L-cysteine concentration at a specified value within its physiologically reasonable range.

2.1.2. Ethanol metabolism

Ethanol metabolism also occurs predominantly in the liver. The ethanol degradation pathways can be classified as three oxidative pathways and one nonoxidative pathway. In this work, the nonoxidative pathway, which produces fatty acid ethyl esters (FAEEs), is not included for it is not closely related to APAP metabolism. The other three distinct human ethanol oxidative pathways are listed in Table 1.

While the first oxidative pathway converts ethanol to acetaldehyde by cytosolic alcohol dehydrogenase (ADH), the second one uses the endoplasmic reticulum microsomal ethanol oxidizing system (MEOS), also known as the cytochrome *P*450 system. This enzyme system is utilized by many pathways of drug metabolism, such as that of APAP. The third pathway oxidizing ethanol to acetaldehyde is catalyzed by peroxisomal catalase. The resulting acetaldehyde, a toxic reactive metabolite, passes into the mitochondrial compartment where it is converted to acetate by mitochondrial aldehyde dehydrogenase. Acetate is then converted to acetyl-CoA and finally oxidized to CO_2 via TCA cycle.

Similar to APAP metabolism, the roles of different metabolic pathways of ethanol can differ. For example, in acute ethanol consumption, ethanol is degraded predominantly by the alcohol dehydrogenase (ADH) mediated pathway. However, under conditions of chronic ethanol consumption, hepatic MEOS activity is enhanced and this pathway can provide a greater contribution to ethanol catabolism than ADH.

2.1.3. Energy metabolism

In addition to APAP and ethanol metabolism, the reactions of glycolysis, TCA cycle, oxidative phosphorylation, and several intracellular transporters are included in the model, as shown in Fig. 1 and listed in Table 1. Both APAP and alcohol metabolism are coupled into these major components of energy metabolism.

2.1.4. Analysis of the overall network

In total, there are 35 metabolites shared among APAP, ethanol and energy metabolism. The major metabolites include

Table 1
Reactions of the hepatic cell model

Index	Enzyme(s)	Identifier	K'_{eq}	Reaction
APAP metabolism				
1.	Cytochrome *P*450 2E1	cyp	2.96E−4 [29]	apap[c]+o2aq[c]+nadpred[c]=napqi[c]+nadpox[c]+h2o[c]
2.	Glucuronyltransferase	glut	2.668 [30]	apap[c]+udpglcur[c]=ag[c]+udp[c]
3.	Sulfotransferase	sult	0.0217 [31]	apap[c]+paps[c]=as[c]+pap[c]
4.	Glutathione-*S*-transferase	gst	1.0E+5 [16]	napqi[c]+glutathionered[c]=asg[c]
5.	Glutathione reductase	glur	56496.51 [16]	napqi[c]+2 glutathionered[c]=apap[c]+glutathioneox[c]
Ethanol metabolism				
6.	Alcohol dehydrogenase	adhE	1.35E−04	ethanol[c]+nadox[c]=acetaldehyde[c]+nadred[c]
7.	Cytochrome *P*450 2E1	p450	1.02E−04	ethanol[c]+nadpred[c]+2 o2aq[c]=acetaldehyde[c]+nadpox[c]+2 h2o2aq[c]
8.	Catalase	catalase	1.00E+08	ethanol[c]+h2o2aq[c]=acetaldehyde[c]+2 h2o[c]
9.	Catalase	catalase	1.00E+08	2 h2o2aq[c]=2 h2o[c]+o2aq[c]
10.	Aldehyde dehydrogenase	ald	4.78E+09	acetaldehyde[m]+nadox[m]+h2o[c]=acetate[m]+nadred[m]
11.	Acetyl coenzyme-A synthetase	acs	0.1166	acetate[m]+atp[m]+coA[m]=acetylcoA[m]+adp[m]+PI[m]
UDPGA biosynthesis				
12.	Phosphoglucomutase	pgm	0.0585	glucose6phos[c]=glucose1phos[c]
13.	UDP-glucose pyrophosphorylase	udp	0.185	glucose1phos[c]+utp[c]=udpg[c]+ppi[c]
14.	Pyrophosphate hydrolysis	pph	2.0E+4	ppi[c]+h2o[c]=2 PI[c]
15.	Nucleoside diphosphokinase	ndk1	11.427	udp[c]+atp[c]=utp[c]+adp[c]
16.	UDP-glucose 6-dehydrogenase	ugd	0.0014 [32]	udpg[c]+2 nadox[c]+h2o[c]=udpglcur[c]+2 nadred[c]
GSH biosynthesis				
17.	Glutathione biosynthesis	gshA	1107.13 [33]	cysteineL[c]+glutamate[c]+glycine[c]+2 atp[c]= glutathionered[c]+2 PI[c]+2 adp[c]
18.	Glutathione reductase (NADPH)	gor	0.0156	glutathioneox[c]+nadpred[c]=2 glutathionered[c]+nadpox[c]
19.	Pyruvate carboxylase	pyr	6.55	atp[m]+pyruvate[m]+co2tot[c]=adp[m]+PI[m]+oxaloacetate[m]
20.	L-cysteine degradation	cys	41.667	cysteineL[c]+o2aq[c]+ketoglutarate[c]+h2o[c]=pyruvate[c]+sulfite[c]+glutamate[c]
21.	Serine biosynthesis	ser	0.01387	pg3[c]+nadox[c]+h2o[c]+glutamate[c]=nadred[c]+PI[c]+ketoglutarate[c]+serineL[c]
22.	Glycine biosynthesis	glyA	3240 [34]	ammonia[c]+co2tot[c]+nadred[m]+serineL[m]=2 glycine[m] +h2o[c]+nadox[m]
23.	Glutamate dehydrogenase (NAD(P)+)	gdh	8.33E+05	glutamate[m]+nadpox[m]+h2o[c]=ketoglutarate[m]+ammonia[c]+nadpred[m]
PAPS biosynthesis				
24.	Sulfite oxidase	sul	5.6	sulfite[c]+o2aq[c]+h2o[c]=sulfate[c]+h2o2aq[c]
25.	Sulfate adenylyltransferase	cysD	1.80E−08	sulfate[c]+atp[c]=ppi[c]+aps[c]
26.	Adenylylsulfate kinase	cysC	1.0E+3 [35]	aps[c]+atp[c]=adp[c]+paps[c]
27.	3′ (2′),5′ -bisphosphate nucleotidase	pap	1.00E+03	pap[c]+h2o[c]=amp[c]+PI[c]
28.	Adenylate kinase	adk	2.7397	atp[c]+amp[c]=2 adp[c]
Glycolysis				
29.	Glucokinase	glk	294	glucose[c]+atp[c]=glucose6phos[c]+adp[c]
30.	Phosphoglucose isomerase	pgi	0.2763	glucose6phos[c]=fructose6phos[c]
31.	Phosphofructokinase	pfk	2290	fructose6phos[c]+atp[c]=fructose16phos[c]+adp[c]
32.	Fructose-1,6-bisphosphatate aldolase	fba	0.0029	fructose16phos[c]=glyceraldehydephos[c]+dihydroxyacetonephos[c]
33.	Triosphosphate Isomerase	tpi	0.0455	dihydroxyacetonephos[c]=glyceraldehydephos[c]
34.	Glycerald-3-P dehydrogenase	gap	0.6119	glyceraldehydephos[c]+PI[c]+nadox[c]=nadred[c]+bpg[c]
35.	Phosphoglycerate kinase	pgk	27.5978	bpg[c]+adp[c]=pg3[c]+atp[c]
36.	Phosphoglycerate mutase 1	gpm	0.0911	pg3[c]=pg2[c]
37.	Enolase	eno	4.2706	pg2[c]=pep[c]+h2o[c]
38.	Pyruvate kinase	pyk	645. 0	pep[c]+adp[c]=pyruvate[c]+atp[c]
TCA cycle				
39.	Pyruvate dehydrogenase	ace	2.189E+5	pyruvate[m]+coA[m]+nadox[m]+h2o[c]=nadred[m]+co2tot[c]+acetylcoA[m]
40.	Citrate synthase	glt	1.14E+6	acetylcoA[m]+oxaloacetate[m]+h2o[c]=coA[m]+citrate[m]
41.	Aconitase	can	0.0684	citrate[m]=citrateiso[m]
42.	Isocitrate dehydrogenase	icd	0.91	citrateiso[m]+nadox[m]+h2o[c]=ketoglutarate[m]+co2tot[c] +nadred[m]
43.	2-Ketoglutarate dehyrogenase	suc1	3.14E+4	ketoglutarate[m]+nadox[m]+coA[m]+h2o[c]=succinylcoA[m]+co2tot[c]+nadred[m]
44.	Succinyl-CoA synthetase	suc2	0.6248	succinylcoA[m]+gdp[m]+PI[m]=gtp[m]+coA[m]+succinate[m]
45.	Succinate dehydrogenase	sdh1	1.0014	succinate[m]+fadenzox[m]=fadenzred[m]+fumarate[m]
46.	Fumarase	fumA	4.2893	fumarate[m]+h2o[c]=malate[m]
47.	Malate dehydrogenase	mdh	1.20E−05	malate[m]+nadox[m]=oxaloacetate[m]+nadred[m]
48.	Nucleoside diphosphokinase	ndk2	0.9615	gtp[m]+adp[m]=gdp[m]+atp[m]
49.	NAD(P)(+) transhydrogenase	pntAB	1.0417	nadpred[c]+nadox[c]=nadpox[c]+nadred[c]

Table 1 (*continued*)

Index	Enzyme(s)	Identifier	K'_{eq}	Reaction
Oxidative phosporylation				
50.	NADH-Q reductase	nuo	21.5857	nadred[m]+ubiquinoneox[c]+4hext=nadox[m]+ubiquinonered[c]
51.	Succinate dehydrogenase complex	sdh2	1.959E−3	fadenzred[m]+ubiquinonered[c]=fadenzox[m]+ubiquinoneox[c]
52.	Cytochrome oxidase	cyo	5.2E+10	2 cytochromecred[c]+0.5 o2aq[c]+4 hext=2 cytochromecox[c]+h2o[c]
53.	F1-ATPase	f1atp	63.347	adp[m]+PI[m]=atp[m]+h2o[c]+3 hext
Intracellular transporers				
54.	Malate–aspartate shuttle 1	mass-1	8.33E+4	oxaloacetate[c]+nadred[c]=malate[c]+nadox[c]
55.	Malate–aspartate shuttle 2	mass-2	1	malate[c]+ketoglutarate[m]=malate[m]+ketoglutarate[c]
56.	Malate–aspartate shuttle 3	mass-3	0.148	oxaloacetate[m]+glutamate[m]=ketoglutarate[m]+aspartate[m]
57.	Malate–aspartate shuttle 4	mass-4	1.20E−05	malate[m]+nadox[m]=oxaloacetate[m]+nadred[m]
58.	Malate–aspartate shuttle 5	mass-5	1	aspartate[m]+glutamate[c]=aspartate[c]+glutamate[m]
59.	Malate–aspartate shuttle 6	mass-6	6.756	aspartate[c]+ketoglutarate[c]=glutamate[c]+oxaloacetate[c]
60.	Malate–aspartate shuttle 7	mass-7	1	nadpox[m]+nadpred[c]=nadpred[m]+nadpox[c]
61.	Pyruvate mito transport	pyr	1	pyruvate[c]=pyruvate[m]
62.	Adenine nucleotide translocase	ant	1	atp[m]+adp[c]=atp[c]+adp[m]
63.	Pi mito–cytosol transport	PIt	1	PI[c]=PI[m]
64.	Glutamate–cytosol transport	glu	1	glutamate[m]=glutamate[c]
65.	SerineL–cytosol transport	ser	1	serineL[c]=serineL[m]
66.	Glycine–cytosol transport	gly	1	glycine[m]=glycine[c]
67.	Acetaldehyde–cytosol transport	acal	1	acetaldehyde[c]=acetaldehyde[m]
68.	Ketoglutarate–cytosol transport	akg	1	ketoglutarate[c]=ketoglutarate[m]
ATP hydrolysis				
69.	ATP use	ATPase	2.0589E+6	atp[c]+h2o[c]=adp[c]+PI[c]
Input and output flux				
70.	APAP			apap[c]=
71.	Ethanol			ethanol[c]=
72.	O_2 uptake			o2aq[c]=
73.	Glucose			glucose[c]=
74.	L-cysteine			cysteineL[c]=
75.	Total CO_2			=co2tot[c]
76.	Ammonia			=ammonia[c]
77.	H_2O			=h2o[c]
78.	AG			=ag[c]
79.	ASG			=asg[c]
80.	AS			=as[c]

Except those references indicated, all other K'_{eq} values are from Alberty's database [10].
[c]: cytosolic compartment; [m]: mitochondrial compartment.

glutathione (GSH), glucose-1-phosphate, acetyl coenzyme A, L-cysteine, pyruvate, glutamate, 3-phosphoglycerate, alpha-ketoglutarate, ATP, ADP, NAD(H), and NADP(H).

In this analysis, five species are assumed to be transported into the system—APAP, ethanol, O_2, glucose and L-cysteine. Six output fluxes are outputs of ammonia, H_2O, AG (APAP glucuronide), ASG (3-(glutathione-*S*-yl)acetaminophen), AS (APAP sulfate) and CO_2. Excluding these 11 transport (input/output) fluxes, there are a total of 69 internal reactions involving 85 species. A total of 24 internal elementary modes (or cycles) are calculated for this network [7]; a total of 13 conserved concentration pools are found by analyzing the stoichiometric structure of the network [8]. Table 3 lists the conserved concentration pools.

Imposing the directions of the external fluxes, each internal flux direction is predicted based on the nonlinear thermodynamic analysis described in Refs. [7] and [9]. In Table 1, all reactions are listed so that the directions of thermodynamically feasible fluxes are left-to-right.

2.2. Thermodynamic data

Thermodynamic constraints acting on metabolite concentrations depend on the standard transformed equilibrium reaction free energies ($\Delta_r G'^{\,0}$) for each participating biochemical reaction. The relationship between reaction free energy and reactant concentrations is expressed as:

$$\Delta_r G' = \Delta_r G'^{\,0} + RT \sum_{i=1}^{n} S_{ij} \ln(C_i) \tag{4}$$

where $\Delta_r G'$ is the Gibbs free energy for a given reaction j; S_{ij} is the stoichiometric coefficient corresponding to species i and reaction j; C_i is the concentration of species i; R is the gas constant; T is the absolute temperature. In this notation, the prime indicates a Legendre transform is used to define Gibbs free energy as a transformed free energy characterized at specified pH, temperature and ionic strength [10]. The transformed Gibbs energy $\Delta_r G'$ provides the criterion for equilibrium and spontaneous changes at the specified condi-

Table 2
List of abbreviations

Abbreviation	Official name
ADP (adp)	Adenosine-diphosphate
AG (ag)	APAP glucuronide
APAP (apap)	*N*-acetyl-*p*-aminophenol, or acetaminophen
AS (as)	APAP sulfate
ASG (asg)	3-(glutathione-*S*-yl)acetaminophen
ATP (atp)	Adenosine-triphosphate
GSH (glutathionered)	Reduced glutathione
GSSH (glutathioneox)	Oxidized glutathione
NAPQI (napqi)	*N*-acetyl-*p*-benzoquinoneimine
NAD (nadox)	Diphosphopyridine nucleotide
NADH (nadred)	Dihydrodiphosphopyridine nucleotide
PAPS (paps)	3′ -phosphoadenylyl-sulfate
PAP (pap)	Adenosine 3′ ,5′ -bisphosphate
T3P1 (glyceraldehydephos)	D-glyceraldehyde-3-phosphate
T3P2 (dihydroxyacetonephos)	Dihydroxy-acetone-phosphate
UDP (udp)	Uridine-diphosphate
UDPGA (udpglcur)	UDP-glucuronic acid
UDPG (udpg)	UDP-D-glucose
UTP (utp)	Uridine-triphosphate
amp	Adenosine-phosphate
aps	Adenosine phosphosulfate
bpg	3-phospho-D-glyceroyl-phosphate
pep	Phosphoenolpyruvate
pg2	2-phosphoglycerate
pg3	3-phosphoglycerate

tions. In this formalism reactants, such as ATP, are treated as a sum of species, i.e. ATP^{4-}, ATP^{3-} and H_2ATP^{2-}. However, variation in free magnesium ion concentration is not considered in this framework, although at different $[Mg^{2+}]$ concentrations, apparent equilibrium constants K'_{eq} may differ by at most a factor of 10 [11].

A thermodynamic database for enzyme-catalyzed reactions undertaken by National Institute of Standards and Technology (NIST) provides an extensive list of experimental measures of thermodynamic information on biochemical reactions in aqueous solutions [6,10]. However, for our purposes, thermodynamic data expressed as standard transformed Gibbs free energies of formation ($\Delta_f G'^{\,0}$) for each reactant are the most straightforward to use. Alberty has provided such a database, which is included in a Mathematica (Wolfrom Research) software package named "BasicBiochemData2", from which equilibrium properties of many reactions can be predicted [10]. For example, the overall GSH biosynthesis reaction is expressed as

$$\begin{aligned}&\text{cysteineL[c]} + \text{glutamate[c]} + \text{glycine[c]} + \text{2atp[c]}\\ &= \text{glutathionered[c]} + \text{2Pi[c]} + \text{2adp[c]}.\end{aligned} \tag{5}$$

It is possible to compute the standard transformed Gibbs free energy ($\Delta_r G'^{\,0}$) for this reaction from the $\Delta_f G'^{\,0}$ values of reactants. Specifically, $\Delta_r G'^{\,0}$ and its corresponding apparent equilibrium constant K'_{eq} are calculated by

$$\Delta_r G'^{\,0} = \sum_{i=1}^{n} S_{ij}\left(\Delta_f G'^{\,0}_i\right) = -RT\ln\left(K'_{eq}\right), \tag{6}$$

where S_{ij} is the stoichiometric number in this biochemical reaction and n is the number of reactants. In this example, $\Delta_f G'^{\,0} = -53.65$, -372.15, -176.08, -2292.50, 637.62, -1059.49 and -1424.70 kJ/mol, respectively, at $T = 298.15$ K, pH = 7 and ionic strength 0.25 M for the species listed in Eq. (5) [10].

Although, in general, the data from Ref. [10] provide a useful estimate of the $\Delta_r G'^{\,0}$ value, predictions from this database do not match experimental data for certain reactions. For the reaction shown in Eq. (5), the computed $\Delta_r G'^{\,0} = 856.11$ kJ/mol and its corresponding apparent equilibrium constant $K'_{eq} = 1.016 \times 10^{-150}$ are not reasonable because experimental measurements estimate $K'_{eq} = 1107.12$ at pH = 7 and ionic strength of 0.25 mM [12]. The reason of this extreme difference is that Alberty's $\Delta_f G'^{\,0}$ values were not constructed to account for the synthetic pathway for GSH ("glutathionered" in Table 1). Although the relative values of Gibbs free energy of formation of GSH and GSSH ("glutathioneox" in Table 1) are reasonable, the absolute values of $\Delta_f G'^{\,0}$ in Ref. [10] are not reasonable relative to other species in the biosynthetic pathway. Based on the experimental K'_{eq} value of Eq. (5) and the GSH/GSSH reduction/oxidation equilibrium thermodynamics, we recalculate the $\Delta_f G'^{\,0}$ values of GSH and GSSH as -235.87 and 346.25 kJ/mol, respectively.

Similarly, there is a large difference in the calculated $\Delta_r G'^{\,0}$ value for Eq. (1), computed as 120.87 kJ/mol, compared to the experimental value of 20.04 kJ/mol [13]. For these reasons, we choose to override the calculated $\Delta_r G'^{\,0}$ and instead use the experimentally measured values if large differences exist.

In addition, for certain reactions we estimate an unknown $\Delta_r G'^{\,0}$ based on thermodynamic cycles present in the reaction network. For example, the overall serine biosynthesis reaction is:

$$\begin{aligned}&\text{pg3[c]} + \text{nadox[c]} + \text{h2o[c]} + \text{glutamate[c]}\\ &= \text{nadred[c]} + \text{Pi[c]} + \text{ketoglutarate[c]} + \text{serineL[c]}.\end{aligned} \tag{7}$$

We find no direct experimental apparent equilibrium constant (K'_{eq}) available for this reaction. However, experi-

Table 3
List of conserved conservation pools

1. nadox[c]+nadred[c]=2 mM	[8]
2. nadox[m]+nadred[m]=2.97 mM	[8]
3. gdp[m]+gtp[m]=10 mM	(*)
4. atp[c]+adp[c]+paps[c]+pap[c]+aps[c]+amp[c]=10 mM	(*)
5. adp[m]+atp[m]=10 mM	[8]
6. fadenzox[m]+fadenzred[m]=1.35 mM	[8]
7. ubiquinonered[c]+ubiquinoneox[c]=1.35 mM	(*)
8. cytochromecox[c]+cytochromecred[c]=1.35 mM	(*)
9. nadpred[c]+nadpox[c]=0.8 mM	[36]
10. nadpred[m]+nadpox[m]=0.8 mM	[36]
11. utp[c]+udpg[c]+udp[c]+udpglcur[c]=10 mM	(*)
12. 3 (coA[m]+acetylcoA[c])+succinylcoA[m]=6 mM	[37]**
13. 3 (atp[c]+glucose6phos[c]+fructose6phos[c]+ 2 fructose16phos[c]+glyceraldehydephos[c]+ dihydroxyacetonephos[c]+PI[c]+2 bpg[c]+pg3[c]+ pg2[c]+pep[c]+glucose1phos[c]+utp[c]+2 ppi[c]− aps[c]−amp[c])−gdp[m]+PI[m]−adp[m]=60 mM	(*)**

*Estimated from simulated data.
**Partition coefficients between cytosol and mitochondria, ε = 3 : 1.

mental K'_{eq} values of 3.10×10^{-6}, 89.5 and 50.0, respectively, are available for the following three reactions [6]:

$$\text{pg3[c]} + \text{nadox[c]} = 3 - \text{phosphohydroxypyruvate[c]} + \text{nadred[c]}, \quad (8)$$

$$3 - \text{phosphonooxypyruvate[c]} + \text{glutamate[c]} = \text{ketoglutarate[c]} + O - \text{phospho} - \text{L} - \text{serine[c]}, \quad (9)$$

$$O - \text{phospho} - \text{L} - \text{serine[c]} + \text{h2o[c]} = \text{serineL[c]} + \text{Pi[c]}. \quad (10)$$

By summing Eqs. (8)–(10), we obtain the overall reaction of Eq. (7). Therefore, the K'_{eq} value for Eq. (7) can be computed from Eqs. (8)–(10). In this case, the value (0.01387) calculated from thermodynamic cycles is close to the value (0.01598) calculated from the Alberty's database [10].

The apparent equilibrium constants for all the reactions in this analysis are listed in Table 1. This thermodynamic dataset represents a cornerstone on which the concentration calculations presented below are based.

2.3. Constraints on the reactant concentrations

In order to be thermodynamically as well as physiologically feasible, the concentrations of all reactants must satisfy a number of constraints based on prior knowledge of metabolism and thermodynamic principles [7,8,14,15]. Tables 3 and 4 list all constraints on reactant concentrations applied in this study.

2.3.1. Concentration pools

Table 3 lists 13 sets of conserved concentration pools for the given network and one set of input/output fluxes. The complete sets of pools are obtained from the left null space of the stoichiometric matrix of the network [8]. For example, because neither NAD nor NADH is transported in or out of the cell, or between the mitochondria and cytosol, the NAD(H) pools are fixed, as indicated by the first two entries in Table 1. The concentration pool values are derived from the references indicated in Table 3.

Table 4
Additional constraints on concentration used in the model

1. All concentrations must be within the range [0.01 M μM, 10 mM].	(*)
2. Thermodynamic constraints:	
a. $\Delta_r G' < 0$ and $\lvert\Delta_r G'\rvert < 75$ kJ/mol, for all i.	(*)
b. $\Delta G'_{ATPase} \in [-60, -50]$ kJ/mol	(*)
c. $\Delta G'_{ndk1}$, $\Delta G'_{ndk2}$ and $\Delta G'_{gdk} \in [-0.001, 0]$ kJ/mol	[8]
3. Fixed concentration or allowable ranges	
a. [glucose]=5.0 mM	[8]
b. [co2tot]=25.0 mM	[8]
c. [o2aq]=0.027 mM	[8]
d. [glutamate]=8.0 mM	[38]
e. [glycine]=3.8 mM	[39]
f. [ammonia]=0.03 mM	[40]
g. [nadred[m]] ∈ [0.3 mM, 2.7 mM]	[8]
h. [apap] ∈ [0.05 mM, 10.0 mM]	[41]
i. [ethanol] ∈ [0.01 mM, 10.0 mM]	[42]
j. [cysteine] ∈ [0.05 mM, 0.5 mM]	[22]
k. [glutathionered] ∈ [0.1 mM, 10.0 mM]	[43]

*Estimated from simulated data.

2.3.2. Thermodynamic constraints

Based on the directions of the boundary (transport) fluxes and the stoichiometry of the reaction network, constraints on flux directions are computed from the feasible thermodynamic behavior of the network [9]. In analyzing this system, it is found that reaction fluxes are predicted to proceed in the positive left-to-right directions as they are listed in Table 1. This information on flux directions translates into constraints on the reaction free energies:

$$\Delta_r G'_j < 0 \text{ for all } j, \quad (11)$$

where j indexes the reactions in the network. Through Eq. (4), Eq. (11) represents a set of constraints on the feasible reactant concentrations. Other constraints imposed are as follows: (1) the ATP hydrolysis potential is enforced at a physiologically reasonable range, $\Delta_r G'_{ATPase} \in [-60, -50]$ kJ/mol; (2) the reactions of ndk1, ndk2 and gdk are assumed to be near equilibrium: $\Delta_r G'_{ndk1}$, $\Delta_r G'_{ndk2}$, $\Delta_r G'_{gdk} \in [-0.001, 0]$ kJ/mol. In addition, based on prior knowledge of metabolite concentrations in the hepatocyte, the typical concentrations or ranges for APAP, ethanol, L-cysteine, glucose, CO_2, O_2, glutamate, GSH, glycine and ammonia are used to reduce the concentration spaces, as outlined in Section 3.

2.4. Metabolic stability constraint

The sets of constraints listed in the previous section define feasible concentration spaces in which the reactant concentrations in the system must fall. However, the resulting feasible spaces are not small enough to make specific predictions of reactant concentrations or metabolic interactions in this system. To reduce the size of the feasible spaces, we define a constraint based on an assumption that metabolic state is stable with respect to the perturbations to the system. Specifically, variations in the thermodynamic state of network in response to changes in substrate concentrations are minimized.

To determine the concentration states for which the system is stable over a variable range of intracellular ethanol concentration, we identify the minimal feasible range of global network free energies over a specific range of ethanol concentration. Defining $\overrightarrow{\Delta_r G'}_{ETOH=0.05\ mM}$ as the vector of free energies at $C_{ETOH}=0.05$ mM, and $\overrightarrow{\Delta_r G'}_{ETOH=10\ mM}$ as the free energies at $C_{ETOH}=10$ mM, the difference in the network free energies for these two states is computed as the difference between these two vectors. Here, the values of 0.05 and 10.0 mM were chosen to represent the typical low and high concentrations of ethanol in the human body, respectively. To minimize feasible ranges of free energy variation, we minimize the objective

$$\Theta^2 = \left\| \overrightarrow{\Delta_r G'}_{ETOH=0.05\ mM} - \overrightarrow{\Delta_r G'}_{ETOH=10\ mM} \right\|^2, \quad (12)$$

by finding optimal values for the reactant concentrations in the system in each of these two states. At the optimal values of

$\overrightarrow{\Delta_r G'}_{\mathrm{ETOH=0.05\ mM}}$ and $\overrightarrow{\Delta_r G'}_{\mathrm{ETOH=10\ mM}}$, which minimize Θ while satisfying the concentration constraints outlined in Section 2.3, it is found that $\Theta = 3.34$ kJ/mol, a value close to RT (2.58 kJ/mol at 37 °C). Using the computed value of Θ as a measure of the maximum allowable variation in the network reaction free energies, we introduce a constraint:

$$\left\| \overrightarrow{\Delta_r G'} - \overrightarrow{\Delta_r G'_m} \right\|^2 \leq \Theta^2, \tag{13}$$

where $\Delta_r G'_m = 1/2\left(\overrightarrow{\Delta_r G'}_{\mathrm{ETOH=0.05\ mM}} + \overrightarrow{\Delta_r G'}_{\mathrm{ETOH=10\ mM}}\right)$ is the mean of the computed free energy vectors that minimizes Θ over the given range of ethanol concentration. By applying the constraint of Eq. (13), it is insured that allowable reaction free energies $\Delta_r G'$ are close to the optimal values computed by maximizing the stability of the network. The impact of applying the constraint of Eq. (13) versus not applying it is illustrated in the following section.

Given the constraints described above, the computational algorithm to predict the metabolic interactions consists of two major steps. The first step is to find out the optimal steady-state that has minimal free energy variations in response to the perturbations in ethanol concentration. Then, using this optimal steady-state as a stability constraint, the second step is to study the impact of the perturbation in ethanol concentration on all reactants by either minimizing or maximizing the total concentration of toxic metabolites in the system.

3. Results

Based on the constructed metabolic network and the compiled thermodynamic data, the thermodynamically feasible

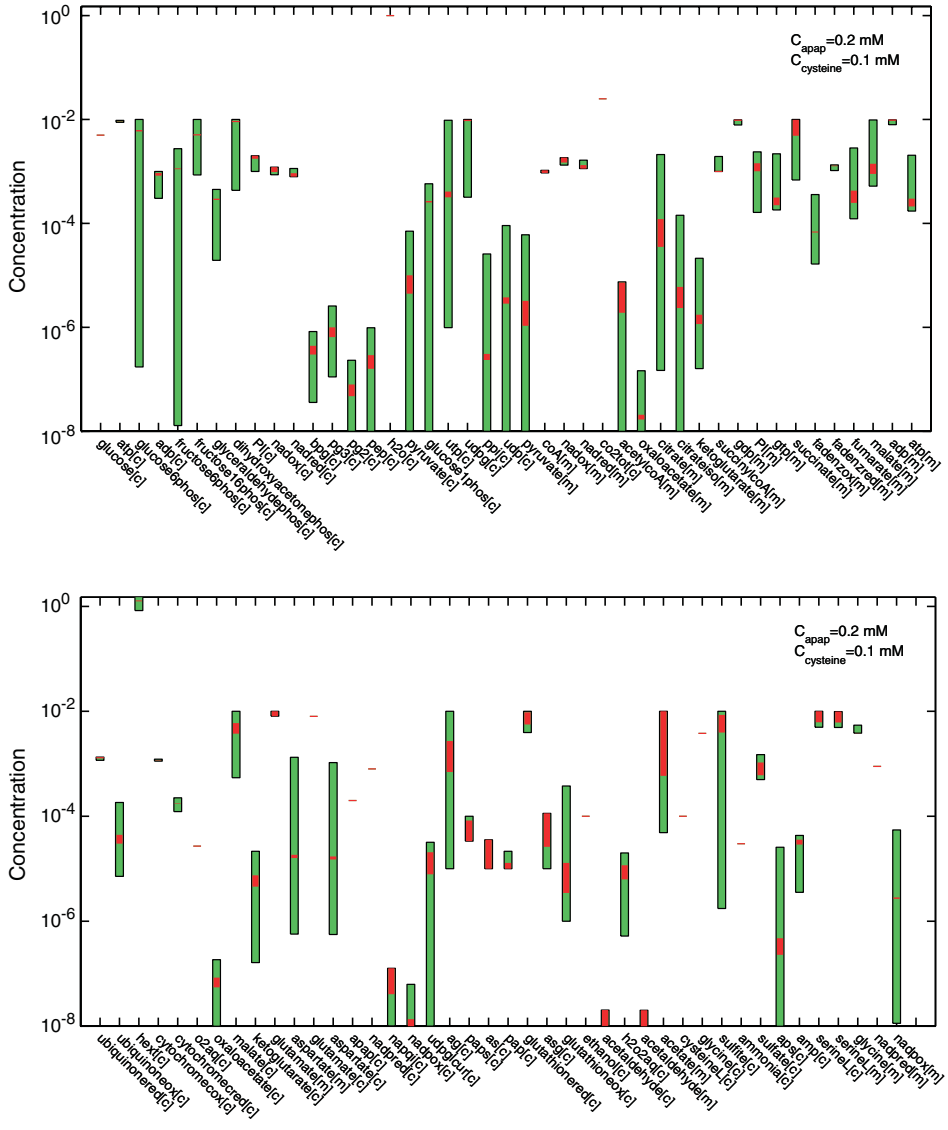

Fig. 2. Feasible concentration ranges for reactants in the model. Green bars indicate the predicted feasible concentration ranges under all constraints detailed in the Methods section and Tables 3 and 4, with the exception of the hypothetical stability constraint of Eq. (13). Red bars indicate the feasible concentration ranges with the additional constraint of Eq. (13). In both calculations, allowable maximum and minimum concentrations for each reactant are used as objective functions. Concentrations of APAP, L-cysteine, ethanol and glucose are fixed at 0.2, 0.1, 0.1 and 5.0 mM, respectively. (For interpretation of the references to colour in this figure legend, the reader is referred to the web version of this article).

concentration ranges for all reactants are calculated with and without the stability constraint of Eq. (13). Non-equilibrium Gibbs free energy for each reaction is predicted at the typical concentration ranges of APAP, ethanol and L-cysteine. Second, the potential impact of ethanol metabolism on APAP toxicity is quantified. Third, the effects of both APAP overdose and fasting on APAP-induced hepatotoxicity are studied.

3.1. Thermodynamically feasible concentration ranges

Before studying the complex interactions between APAP and ethanol, it is useful to profile the thermodynamically feasible concentration range for each reactant. To do this, the allowable maximum and minimum concentrations under the thermodynamic and physiological constraints are computed. Fig. 2 plots the feasible concentration range of each metabolite in the system, computed with glucose, APAP, L-cysteine, and ethanol concentrations fixed at 5.0, 0.2, 0.1 and 0.1 mM, respectively. Green bars indicate the feasible ranges predicted using all constraints but the hypothetical stability constraint of Eq. (13); the red bars indicate the feasible ranges when the hypothetical stability constraint is included. When Eq. (13) is satisfied, the feasible concentration ranges are dramatically reduced compared to when Eq. (13) is not applied.

Comparison of predicted and experimentally observed concentrations provides a validation of the compiled set of thermodynamic data. For example, the calculated concentration range for NAPQI is of the order of 10^{-7} M, which matches with experimental observations [16]. Thus, the compiled apparent equilibrium constants for reaction 1 and 5 are reasonable. In addition, these calculations also provide the estimates of some reactant concentrations that are experimentally difficult to measure. For example, the predicted concentration range of PAPS is relatively narrow and centered around 75 μM.

3.2. Ethanol and acetaminophen metabolic interaction

In this section, the behavior of the metabolic network is profiled by minimizing the total concentration of toxic intermediate species, given the set of constraints defined above. This calculation finds the biologically optimal operational point for the network—a state at which concentrations of acetaldehyde, H_2O_2 and NAPQI are minimized. Because the concentration ranges for these reactants vary by several orders of magnitude, the objective is formulated by summing the logarithms of reactant concentration:

$$\text{objective} = \log(C_{\text{acetal}}) + \log(C_{H_2O_2}) + \log(C_{\text{NAPQI}}). \qquad (14)$$

Plotted in Fig. 3A are the relative concentrations of NAD, predicted by minimizing the objective of Eq. (14), as a function of ethanol concentration. NAD concentrations shown in this plot are relative to the amounts predicted at $C_{\text{ETOH}}=0.05$ mM. For these results, APAP, L-cysteine, and glucose are set at 0.2, 0.1 and 5.0 mM, respectively. Ethanol oxidation via alcohol dehydrogenase and acetaldehyde dehydrogenase consumes NAD and generates NADH. Mitochondria NAD level is

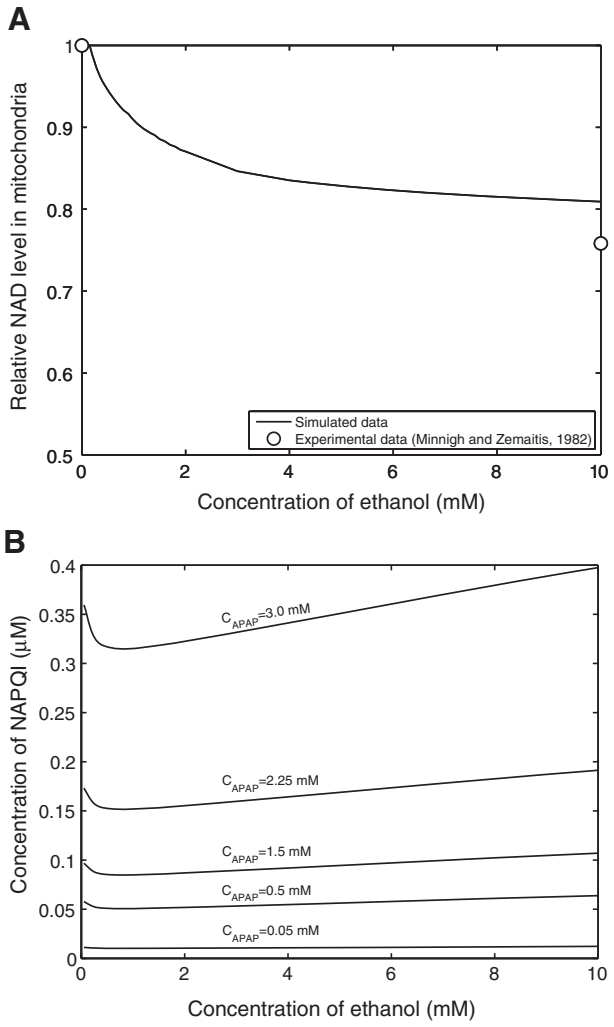

Fig. 3. Changes of redox state in mitochondria and NAPQI level response to ethanol. A. Predicted relative concentrations of NAD in mitochondria are plotted as a function of intracellular ethanol. Plotted concentrations are relative to the concentration at $C_{\text{ETOH}}=0.05$ mM. As ethanol concentration increases, NAD is consumed and NADH is built up. Therefore, NAD/NADH systems become increasingly reduced. Experimental data shown in the plot are from Ref. [17]. B. Predicted concentrations of NAPQI are plotted as a function of ethanol concentration for C_{APAP} values ranging from 0.05 to 3.0 mM. Concentrations in A and B are computed using the objective function of Eq. (14). Concentrations of L-cysteine and glucose are fixed at 0.1 and 5.0 mM, respectively.

reported to decrease by nearly 25% when ethanol concentration is increased from 0 to 10 mM in isolated hepatocytes [17]. The data from Ref. [17] are plotted as open circles in Fig. 3A. It should be emphasized that the simulation is not adjusted to fit the experimental data—there are no arbitrarily free parameters in the model. The predicted relationship between NAPQI and ethanol is plotted in Fig. 3B for different concentrations of APAP. The NAPQI concentration increases dramatically with increasing APAP, and varies less with ethanol concentration.

The impact of increasing ethanol concentration on the three pathways of APAP metabolism is examined in Fig. 4. Fig. 4A plots the predicted relative GSH, PAPS and UDPGA concentrations as a function of ethanol concentration at fixed APAP concentration of 0.2 mM. Values on the vertical axis are

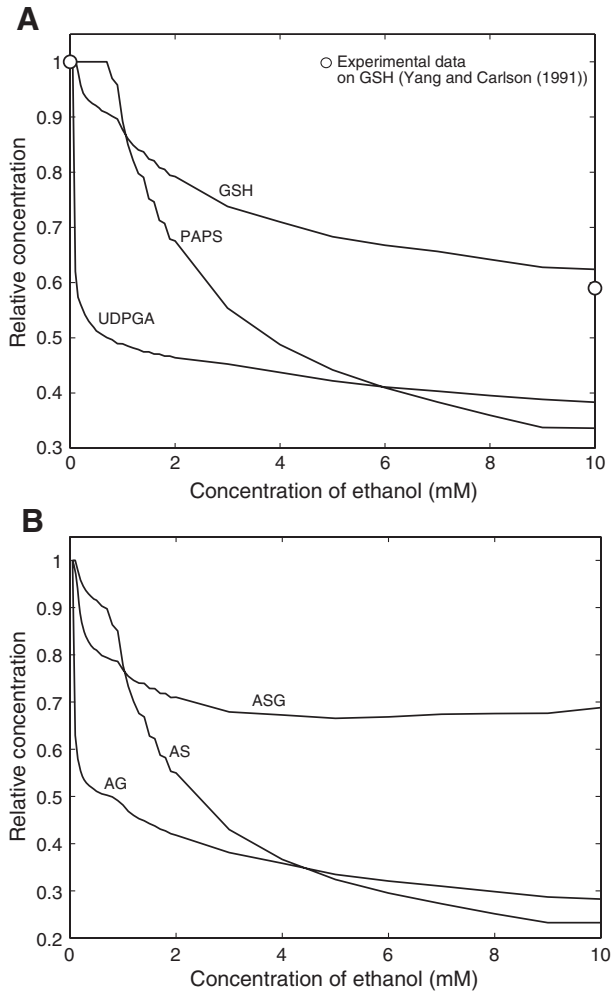

Fig. 4. The impact of ethanol concentration on the three pathways of APAP metabolism. A. It shows the predicted relative GSH, PAPS and UDPGA concentrations as a function of ethanol concentration at fixed APAP concentration of 0.2 mM. Values on the vertical axis are expressed as concentrations relative to the amounts predicted at C_{ETOH}=0.05 mM. Experimental data used in this plot is from Ref. [18]. B. The corresponding products for these pathways, ASG, AS and AG, are diminished with increasing ethanol in a manner similar to GSH, PAPS, and UDPGA. Concentrations of APAP, L-cysteine and glucose in A and B are fixed at 0.2, 0.1 and 5.0 mM, respectively. Objective function of Eq. (14) is used to compute the relative concentrations in A and B.

concentrations relative to the amounts predicted at C_{ETOH}= 0.05 mM. Relative concentrations of these three species, which are substrates for the glutathione conjugation, sulfation, and glucuronidation pathways, are predicted to diminish with increasing ethanol. At high ethanol concentration (10 mM), these species are depleted to 60% (GSH), 35% (PAPS), and 40% (UDPGA) of their concentrations at C_{ETOH}=0.05 mM. Yang and Carlson [18] report that ethanol intake (4 g/kg) in the male Sprague–Dawley rats reduces hepatic GSH from 7.0 to 4.17 mol μmol/g tissue, which corresponds to a 59.6% depletion in hepatic GSH. These experimental data match the predicted data as shown in Fig. 4A. The corresponding products for these pathways, ASG, AS and AG, are diminished with ethanol in a similar manner, as illustrated in Fig. 4B.

The UDPGA pathway is predicted to be the most sensitive to ethanol dose because both ethanol metabolism and the APAP glucuronidation pathway use NAD as a substrate. Glucuronidation competes with ethanol metabolism for NAD and the increasing ratio of NADH/NAD depresses the synthesis of UDPGA. As a result, increasing concentrations of ethanol is predicted to drive APAP metabolism toward the sulfation pathway and the GSH conjugation pathway, which potentially produce the major toxic metabolite NAPQI.

The simulated data also show that at the low ethanol concentration the magnitude of depletion of PAPS is less than that of UDPGA and GSH. Yet at high ethanol concentration, the PAPS concentration continues to decline to a relative level lower than that of GSH and UDPGA. This behavior is explained by the inhibition of biosynthesis of PAPS by ethanol. Synthesis of PAPS requires sulfate as a sulfur-donor and consumes two ATP (see reactions 25 and 26 in Table 1). Because the sulfate source, L-cysteine, is fixed at its typical concentration (0.1 mM), the amount of ATP available for PAPS synthesis is critical. However, degradation of ethanol also consumes ATP in converting acetate into acetyl-CoA (reaction 11) while inhibiting TCA cycle and ATP production [19]. Therefore, the increasing ethanol concentration results in a diminished potential to synthesize PAPS.

Fig. 4A shows that the impact of ethanol concentration on the glutathione pathways is less than on the others. This behavior may result from the lack of competition between GSH synthesis and ethanol metabolism via NAD/NADH system. Specifically, a complete degradation of one ethanol molecule consumes 5 NAD (1 for ethanol dehydrogenase, 1 for acetaldehyde dehydrogenase, and 3 for TCA cycle), while GSH synthesis generates no net NADH reducing equivalents (reactions 21 and 22 in Table 1). On the other hand, both the cytochrome *P*450 pathway and glutathione reductase (reactions 1 and 18 in Table 1) consume one NADPH. Subsequently, these two pathways compete for NADPH reducing equivalents. Yet the competition for NADPH is alleviated by glutamate dehydrogenase (reaction 23) which produces NADPH. Nevertheless, ethanol degradation and GSH synthesis compete for ATP (reactions 11 and 17), resulting in a reduction of GSH level with increasing ethanol.

In sum, consuming ethanol increases the overall reduced state of the metabolic system, inhibits the ATP production, and decreases biosyntheses of GSH, PAPS and UDPGA. These changes lead to an increase in NAPQI formation (shown in Fig. 3B) and a decrease in NAPQI detoxification, resulting in accumulation of NAPQI. As a result, chronic alcoholics are more sensitive to APAP dose than nonalcoholics. In addition, predicted concentrations of other toxic metabolites, acetaldehyde and H_2O_2, increase with ethanol concentrations (results not shown).

3.3. Effects of APAP overdose

At therapeutic doses, hepatic metabolism eliminates over 95% of APAP to glucuronide conjugates (AG) and sulfate conjugates (AS). The remainder (<5%) may generate reactive

metabolites (NAPQI). However, the sulfate and glucuronide pathways are capacity-limited. Consequently, in overdose the relative flux through the cytochrome *P*450 system increases and there is an increased demand for hepatocellular glutathione to detoxify NAPQI. Thus the availability of glutathione becomes critical in the case of APAP overdose.

Fig. 5A shows the predicted optimal GSH concentrations in response to the increasing ethanol concentration for APAP concentrations ranging from 0.05 to 5.0 mM. The feasible concentration of GSH is found to be about 10 mM at C_{ETOH}=0.05 mM, and GSH is depleted to 4.3 mM under the combined effects of APAP overdose and ethanol intake. This result indicates that glutathione pool is sensitive to APAP intake in chronic alcoholism, even at low levels of APAP.

Fig. 5B shows that available GSH drops substantially at a fixed ethanol concentration of 5.0 mM, even at relatively low APAP concentrations. GSH concentration is reduced from 10.0 to 5.5 mM when APAP concentration is changed from 0.05 to 1.0 mM. Fig. 5C shows a two-dimensional contour plot of predicted GSH as a function of APAP and ethanol concentration. Note that the predicted sensitivity of GSH to APAP is greater than that to ethanol concentration. Concentrations of APAP up to 1.0 mM are considered non-toxic based on Rumack–Matthew Nomogram [20]. However, our results indicate that when ethanol is present, even a therapeutic dose (about 0.1 mM) of APAP could drive GSH concentration to below 65% of its value at C_{APAP}=0.05 mM. With diminished GSH concentration, NAPQI detoxification would be slowed. In fact, animal studies indicate that even at non-toxic doses of APAP, GSH could be depleted by 70% or more in chronic alcoholism [21]. Note that model predictions presented here are based on the best-case predication that minimizes the toxic intermediates.

Similar to GSH, the PAPS level is depleted with the increasing concentration of ethanol, as shown in Fig. 6. Fig. 6A shows predicted PAPS concentrations versus intracellular ethanol for different levels of APAP concentration. The model predicts that PAPS is diminished more than GSH in response to the increasing APAP level. At C_{ETOH}=5.0 mM, PAPS drops from approximately 0.1 mM at C_{APAP}=0.05 mM to below 0.04 mM at C_{APAP}=0.5 mM, corresponding to a 60% reduction in available PAPS. Therefore, the sulfation pathway is predicted to be severely inhibited by even low concentrations of APAP. This drop in PAPS is also demonstrated in Fig. 6B where PAPS concentrations are plotted as a function of APAP at a constant ethanol concentration (5.0 mM). A 50% decrease in the predicted PAPS concentration occurs at approximately 0.1 mM APAP concentration. Thus, the PAPS concentration is highly sensitive to therapeutic APAP concentrations because of the interactions with the ethanol detoxification pathways. Fig. 6C shows the contour plot of predicted PAPS concentration as a function of C_{ETOH} and C_{APAP}. Predicted PAPS level is significantly more sensitive to APAP than to intracellular ethanol.

As a result of the depletion of GSH and PAPS, the predicted concentration of NAPQI increases approximately 65 times when C_{APAP} is increased from 0.05 to 3.0 mM at the fixed

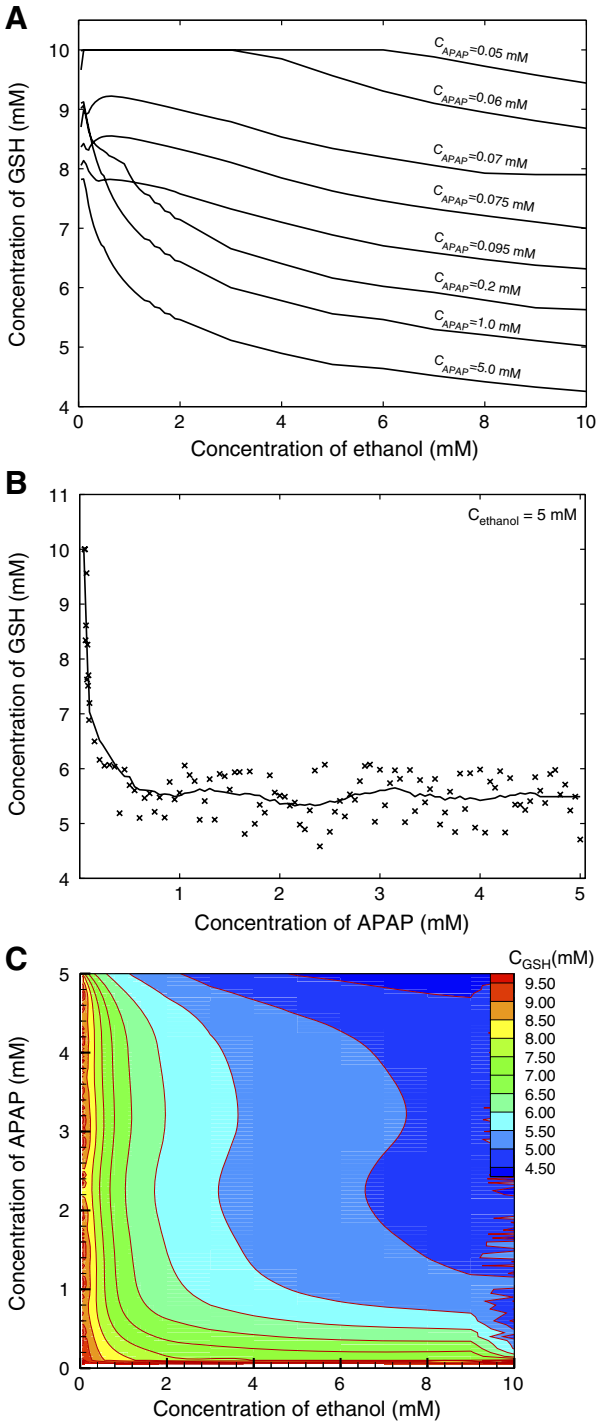

Fig. 5. Illustration of predicted effects of both APAP overdose and ethanol intake on GSH level in the hepatocyte. A. It shows the predicted optimal GSH concentrations in response to the increasing ethanol concentration for APAP concentrations ranging from 0.05 to 5.0 mM. B. At a specified ethanol concentration 5.0 mM, available GSH drops substantially even at relatively low APAP concentrations. C. The two-dimensional contour plot of predicted GSH as a function of APAP and ethanol concentrations is shown. The predicted sensitivity of GSH to APAP is greater than that to ethanol concentration at low concentrations of APAP and ethanol. The wiggled curves shown in Fig. 5B at the high ethanol concentrations are caused by the non-smooth constructed space in the optimization process. In A, B and C, concentrations of L-cysteine and glucose are fixed at 0.1 and 5.0 mM, respectively. The contour plot was drawn using the software Tecplot (www.tecplot.com).

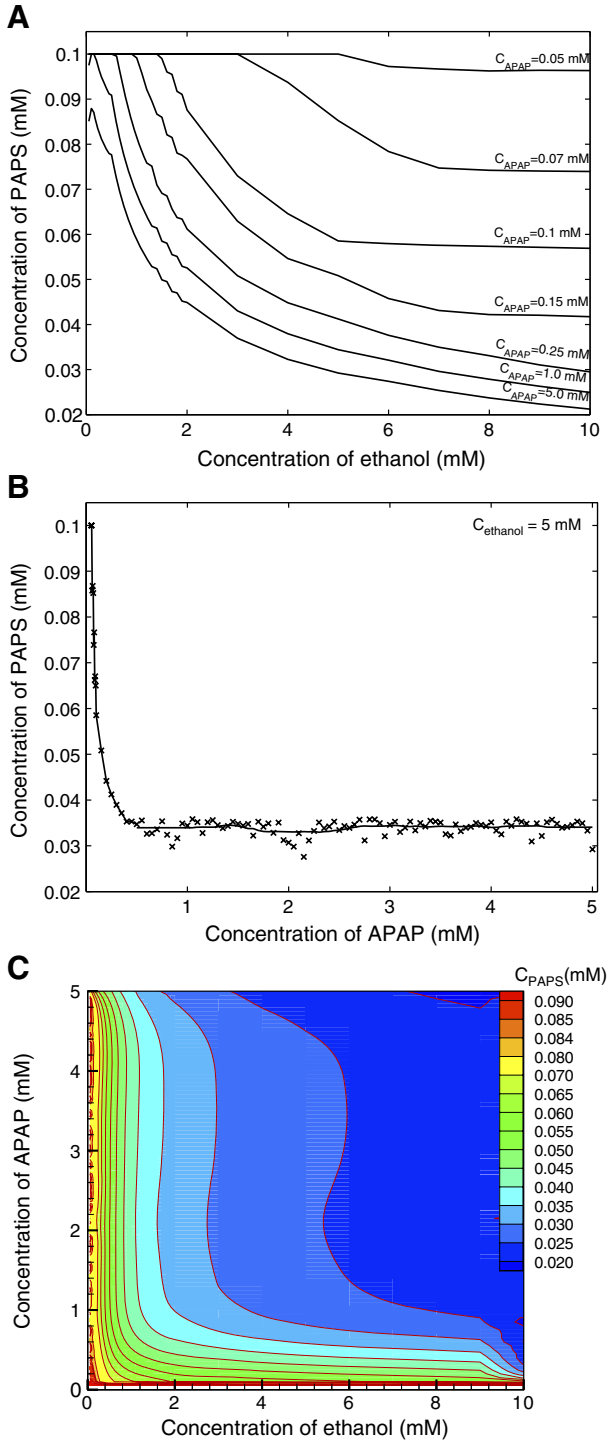

Fig. 6. Illustrations of predicted effects of both APAP overdose and ethanol intake on PAPS level in the hepatocyte. A. It shows the predicted PAPS concentrations versus intracellular ethanol for different levels of APAP concentration. B. PAPS concentrations are plotted as a function of APAP at a fixed ethanol concentration (5.0 mM). The model predicts that PAPS is diminished more than GSH in response to the increasing in APAP level. C. It shows the contour plot of predicted PAPS concentrations as a function of both C_{ETOH} and C_{APAP}. Predicted PAPS level is more sensitive to APAP than to intracellular ethanol. In A, B and C, concentrations of L-cysteine and glucose are fixed at 0.1 and 5.0 mM, respectively. The contour plot was drawn using the software Tecplot (www.tecplot.com).

ethanol concentration of 5.0 mM, as shown in Fig. 3B. However, no significant effects on acetaldehyde or H_2O_2 are found with the increasing APAP concentrations.

3.4. Effects of fasting on APAP-induced hepatotoxicity

Short-term fasting and severe malnutrition also contribute to APAP-induced hepatotoxicity. Their effects on APAP metabolism are even more significant than those of ethanol [2]. Fasting decreases the capacity of hepatic conjugation of APAP by depleting the hepatic glutathione reserves and reducing the UDPGA concentration [2]. As a result, more APAP is metabolized by CYPs, thus the level of toxic NAPQI is increased.

Therefore, any promotion of hepatic GSH synthesis may prevent APAP-induced hepatic injury. It is known that the rate of GSH synthesis is primarily dependent on the availability of intracellular L-cysteine [22]. Evidence also comes from the fact that *N*-acetylcysteine (NAC) is an effective antidote for APAP toxicity by providing a sulfhydryl donor for glutathione synthesis, and enhancing the sulfation pathway for the conjugation of NAPQI [23]. Thus, it is possible to study both fasting and NAC effects on APAP metabolism by varying L-cysteine concentrations.

Fig. 7 shows the levels of GSH, PAPS and UDPGA available as a function of intracellular L-cysteine concentrations. Values in vertical axis are concentrations relative to the amounts predicted at 0.08 mM L-cysteine. It is apparent that with increasing concentration of L-cysteine, the capacity to metabolize APAP increases because the predicted GSH and PAPS concentrations increase. The model predictions show that GSH concentration continuously grows over the reasonable range of L-cysteine concentration, and the PAPS level

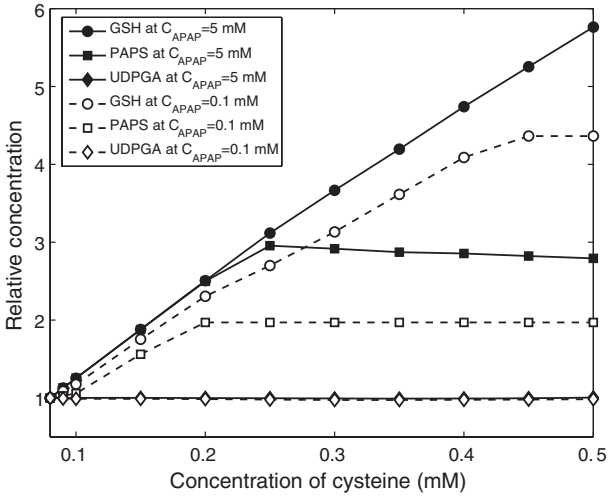

Fig. 7. The levels of GSH, PAPS and UDPGA available as a function of intracellular L-cysteine concentration. Values on the vertical axis are expressed as concentrations relative to the amounts predicted at $C_{cysteine}=0.08$ mM. The solid line represents the toxic level of APAP (5.0 mM); the dashed line represents the non-toxic level of APAP (0.1 mM). As L-cysteine concentration increases, the capacity to metabolize APAP increases for the predicted GSH and PAPS concentrations increase. However, the constraint-based model predicts little effect of L-cysteine on UDPGA concentration. Glucose and ethanol concentrations are fixed at 5.0 and 0.15 mM, respectively.

becomes saturated because of active constraints on ATP and ADP. The constraint-based model predicts little effects of L-cysteine concentration on UDPGA concentrations. It is predicted that L-cysteine has a greater impact on PAPS and GSH at the toxic dose (5.0 mM) of APAP than at non-toxic dose (0.1 mM). The PAPS concentration increases about 300% over the studied range of C_{cysteine} at toxic level of APAP, compared to the 200% increase observed at non-toxic levels of APAP. In other words, the impact of L-cysteine on GSH and PAPS concentrations is enhanced at high levels of APAP. Thus, increasing APAP from non-toxic to toxic levels may promote PAPS and GSH syntheses. This behavior has been observed in cultured rat hepatocytes in which glutathione has been depleted by DEM (diethyl maleate) [24]. At low levels of APAP, both PAPS and GSH concentrations are saturated for L-cysteine concentration greater than approximately 0.45 mM. In both cases (non-toxic or toxic levels of APAP), hepatic GSH level tends to parallel hepatic L-cysteine concentrations, which matches the observation that in liver of rats fed sulfur amino acid-supplemented diets, the GSH level is much higher than in liver of rats fed an unsupplemented low protein diet [22].

4. Discussion

In sum, we have constructed a metabolic network that includes APAP, ethanol, and energy metabolism, and identified intermediate metabolites directly shared among these pathways. Thermodynamic data such as equilibrium constants and Gibbs free energies of formation have been compiled. Based on the constructed reaction network and the compiled thermodynamic data, systematic studies on interactions in APAP-induced hepatotoxicity were conducted and the simulated results were compared to the experimental observations.

In essence, a thermodynamically based method has been developed to systemically study drug metabolism and drug–drug metabolic interactions. The major advantages of this thermodynamically based analysis are: (1) it reveals metabolic interactions on a global network scale. Traditional methods to study drug interactions, such as between APAP and ethanol, focus on one or few metabolic pathways. For example, some focus on the glucuronidation pathway [2]; others on both the sulfation and glucuronidation pathways [25,26]; and others on the GSH conjugation pathways [27,28]. It is experimentally difficult to measure fluxes and concentrations in all of these pathways simultaneously and thus their complicated interactions can not be explained on the network scale. Here, we have attacked the network-scale problem computationally. (2) There are no arbitrarily adjustable parameters involved in this study. All data used in this model are based on either available experimental measures, such as the data listed in Tables 3 and 4, or thermodynamic data calculated from corresponding experiments, such as the equilibrium constants listed in Table 1. None of these data are model-dependent. (3) Modeling results are straightforward compared to experimental results since the method developed here predicts metabolite concentrations, rather than reaction fluxes. Although many flux-based analytic methods are available for biochemical reaction networks, associated modeling results may be difficult to directly compare to experimental results. In this work, the predicted feasible concentration ranges for cases where the cellular concentrations are known provide direct validations of our modeling methodology. Computational modeling predicts that the non-toxic pathways for APAP metabolism and the pathway for detoxifying NAPQI are inhibited by network interactions with ethanol metabolism. Specifically, the PAPS pathway is predicted to be highly sensitive to even therapeutic doses of APAP when ethanol is present.

Based on this framework, multiple phenomena may be simulated, such as the effects of simultaneously varying APAP, L-cysteine, glucose, and ethanol concentrations rather than considering one variable at a time. In addition, explicit consideration of the oxidative stress (reactive oxygen species) rather than using overall concentration of total toxic metabolites may be possible. The approach may allow us to characterize the effects of multiple CYP-inducing drugs that may enhance APAP-induced hepatotoxicity, and the effects of cellular pH on the biochemical reaction network. Nevertheless, this approach has the major limitation of unable to capture the time-dependent behaviors such as the opposite effects of acute versus chronic alcohol intake on hepatotoxicity. Future analysis in this area will require kinetic information be incorporated into the model. In this case, thermodynamic constraints developed in this work may provide additional constraints on the dynamic models. As further knowledge becomes available, particularly on the hepatic cytochrome *P*450 enzyme kinetics, the model can be expanded to include these details.

In sum, this work has demonstrated the potential utility of thermodynamically based profiling of metabolic network interactions in screening of drug candidates and analysis of potential toxicity. By providing predictions of key metabolite concentrations as a function of the two drug concentrations (see Figs. 5 and 6), we are able to predict the simultaneous action of these interacting drugs on the network function. Given established network structure (metabolic reaction stoichiometry), drug–drug interactions of arbitrary complexity may be screened computationally. The results of such computational screenings may be used to steer experimental investigations to verify and refine the models. For example, by identifying which species are likely to be the most sensitive to the concentrations of interacting drugs, the computational results may suggest targeted experiments to uncover mechanisms of metabolic interaction. In addition, the ability to predict significant drug–drug interaction could be potentially useful in identifying putative interactions impacting drug efficiency and/or toxicity before such effects are observed clinically.

Acknowledgement

This work was supported by NIH grant GM068610.

References

[1] P. Draganov, et al., Alcohol–acetaminophen syndrome. Even moderate social drinkers are at risk, Postgrad. Med. 107 (1) (2000) 189–195.

[2] V.F. Price, D.J. Jollow, Mechanism of decreased acetaminophen glucuronidation in the fasted rat, Biochem. Pharmacol. 37 (6) (1988) 1067–1075.
[3] C. Sato, M. Nakano, C.S. Lieber, Prevention of acetaminophen-induced hepatotoxicity by acute ethanol administration in the rat: comparison with carbon tetrachloride-induced hepatoxicity, J. Pharmacol. Exp. Ther. 218 (3) (1981) 805–810.
[4] T.M.a.K.Y. Isao Sumioka, Acetaminophen-induced hepatotoxicity: still an important issue, Yonago Acta Med. (47) (2004) 17–28.
[5] R.A. Alberty, A short history of the thermodynamics of enzyme-catalyzed reactions, J. Biol. Chem. 279 (27) (2004) 27831–27836.
[6] R.N. Goldberg, Y.B. Tewari, T.N. Bhat, Thermodynamics of enzyme-catalyzed reactions—a database for quantitative biochemistry, Bioinformatics 20 (16) (2004) 2874–2877.
[7] D.A. Beard, et al., Thermodynamic constraints for biochemical networks, J. Theor. Biol. 228 (3) (2004) 327–333.
[8] D.A. Beard, H. Qian, Thermodynamic-based computational profiling of cellular regulatory control in hepatocyte metabolism, Am. J. Physiol:. Endocrinol. Metab. 288 (3) (2005) E633–E644.
[9] F. Yang, H. Qian, D.A. Beard, Ab initio prediction of thermodynamically feasible reaction directions from biochemical network stoichiometry, Metab. Eng. 7 (4) (2005) 251–259.
[10] R.A. Alberty, Thermodynamics of Biochemical Reactions, Wiley Higher Education, 2003.
[11] R.A. Alberty, Equilibrium calculations on systems of biochemical reactions at specified pH and pMg, Biophys. Chemist. 42 (2) (1992) 117–131.
[12] P. Apontoweil, W. Berends, Glutathione biosynthesis in *Escherichia coli* K 12. Properties of the enzymes and regulation, Biochim. Biophys. Acta 399 (1) (1975) 1–9.
[13] Y. Motokawa, G. Kikuchi, Glycine metabolism in rat liver mitochondria: V. Intramitochondrial localization of the reversible glycine cleavage system and serine hydroxymethyltransferase, Arch. Biochem. Biophys. 146 (2) (1971) 461–464.
[14] H. Qian, D.A. Beard, Thermodynamics of stoichiometric biochemical networks in living systems far from equilibrium, Biophys. Chemist. 114 (2–3) (2005) 213–220.
[15] H. Qian, D.A. Beard, S.D. Liang, Stoichiometric network theory for nonequilibrium biochemical systems, Eur. J. Biochem. 270 (3) (2003) 415–421.
[16] D.W. Potter, J.A. Hinson, Reactions of *N*-acetyl-*p*-benzoquinone imine with reduced glutathione, acetaminophen, and NADPH, Mol. Pharmacol. 30 (1) (1986) 33–41.
[17] M.B. Minnigh, M.A. Zemaitis, Altered acetaminophen disposition in fed and food-deprived rats after acute ethanol administration, Drug Metab. Dispos. 10 (2) (1982) 183–188.
[18] C.M. Yang, G.P. Carlson, Effects of ethanol on glutathione conjugation in rat liver and lung, Biochem. Pharmacol. 41 (6–7) (1991) 923–929.
[19] L.E. Nagy, Molecular aspects of alcohol metabolism: transcription factors involved in early ethanol-induced liver injury, Annu. Rev. Nutr. 24 (2004) 55–78.
[20] S. Vassallo, A.N. Khan, M.A. Howland, Use of the Rumack–Matthew nomogram in cases of extended-release acetaminophen toxicity, Ann. Intern. Med. 125 (11) (1996) 940.
[21] J.R. Tucker, Late-presenting acute acetaminophen toxicity and the role of *N*-acetylcysteine, Pediatr. Emerg. Care 14 (6) (1998) 424–426.
[22] C. Cresenzi, J. Lee, M. Stipanuk, Cysteine is the metabolic signal responsible for dietary regulation of hepatic cysteine dioxygenase and glutamate cysteine ligase in intact rats, J. Nutr. 133 (9) (2003) 2697–2702.
[23] L.P. James, P.R. Mayeux, J.A. Hinson, Acetaminophen-induced hepatotoxicity, Drug Metab. Dispos. 31 (12) (2003) 1499–1506.
[24] K. Dalhoff, H.E. Poulsen, Simultaneous measurements of glutathione and activated sulphate (PAPS) synthesis rates and the effects of selective inhibition of glutathione conjugation or sulphation of acetaminophen, Biochem. Pharmacol. 46 (3) (1993) 383–388.
[25] R.E. Kane, A.P. Li, D.R. Kaminski, Sulfation and glucuronidation of acetaminophen by human hepatocytes cultured on Matrigel and type 1 collagen reproduces conjugation in vivo, Drug Metab. Dispos. 23 (3) (1995) 303–307.
[26] S. Fayz, et al., Inhibition of acetaminophen sulfation by 2,6-dichloro-4-nitrophenol in the perfused rat liver preparation. Lack of a compensatory increase of glucuronidation, Drug Metab. Dispos. 12 (3) (1984) 323–329.
[27] J.M. Hassing, H. Rosenberg, S.J. Stohs, Acetaminophen-induced glutathione depletion in diabetic rats, Res. Commun. Chem. Pathol. Pharmacol. 25 (1) (1979) 3–11.
[28] J.P. Richie Jr., C.A. Lang, T.S. Chen, Acetaminophen-induced depletion of glutathione and cysteine in the aging mouse kidney, Biochem. Pharmacol. 44 (1) (1992) 129–135.
[29] K.E. Thummel, et al., Oxidation of acetaminophen to *N*-acetyl-*p*-aminobenzoquinone imine by human CYP3A4, Biochem. Pharmacol. 45 (8) (1993) 1563–1569.
[30] V.F. Price, D.J. Jollow, Increased resistance of diabetic rats to acetaminophen-induced hepatotoxicity, J. Pharmacol. Exp. Ther. 220 (3) (1982) 504–513.
[31] D.J. Sweeny, L.A. Reinke, Sulfation of acetaminophen in isolated rat hepatocytes. Relationship to sulfate ion concentrations and intracellular levels of 3′ -phosphoadenosine-5′ -phosphosulfate, Drug Metab. Dispos. 16 (5) (1988) 712–715.
[32] J.J. Hjelle, Hepatic UDP-glucuronic acid regulation during acetaminophen biotransformation in rats, J. Pharmacol. Exp. Ther. 237 (3) (1986) 750–756.
[33] R.B. Johnston, K. Bloch, Enzymatic synthesis of glutathione, J. Biol. Chem. 188 (1) (1951) 221–240.
[34] T. Sato, et al., Glycine metabolism by rat liver mitochondria: I. Synthesis of two molecules of glycine from one molecule each of serine, bicarbonate and ammonia, J. Biochem. (Tokyo) 65 (1) (1969) 63–70.
[35] D.C. Medina, et al., Temperature effects on the allosteric transition of ATP sulfurylase from *Penicillium chrysogenum*, Arch. Biochem. Biophys. 393 (1) (2001) 51–60.
[36] T. Fukuwatari, et al., Effects of fatty liver induced by niacin-free diet with orotic acid on the metabolism of tryptophan to niacin in rats, Biosci. Biotechnol. Biochem. 66 (6) (2002) 1196–1204.
[37] N.J. Faergeman, J. Knudsen, Role of long-chain fatty acyl-CoA esters in the regulation of metabolism and in cell signalling, Biochem. J. 323 (Pt 1) (1997) 1–12.
[38] T. Planche, et al., Plasma glutamine and glutamate concentrations in Gabonese children with *Plasmodium falciparum* infection, QJM 95 (2) (2002) 89–97.
[39] R.K. Hampson, M.K. Taylor, M.S. Olson, Regulation of the glycine cleavage system in the isolated perfused rat liver, J. Biol. Chem. 259 (2) (1984) 1180–1185.
[40] T. Okamoto, K.Y. Nakakura, H. Saito, Y. Hashimoto, K. Mitsubayashi, Development of the ammonia bio-sniffer with FMO3, 2004 Joint International Meeting of 206th Meeting of the Electrochemical Society and 2004 Fall Meeting of the Electrochemical Society of Japan, The Electrochemical Society, Inc., Honolulu, USA, 2004.
[41] W.F. Schwenk, J.C. Kahl, Acetaminophen glucuronidation accurately reflects gluconeogenesis in fasted dogs, Am. J. Physiol. 271 (3 Pt 1) (1996) E529–E534.
[42] C.S. Lieber, Alcohol and the liver: metabolism of alcohol and its role in hepatic and extrahepatic diseases, Mt. Sinai J. Med. 67 (1) (2000) 84–94.
[43] S. Lu, Regulation of hepatic glutathione synthesis: current concepts and controversies, FASEB J. 13 (10) (1999) 1169–1183.